INCORPORATING A PRIORI KNOWLEDGE INTO A MOVING VEHICLE DETECTOR FOR TERRASAR-X DATA

A. Laika[1)], F. Meyer[2)], S. Hinz[1)], R. Bamler[1,2)]

1) Remote Sensing Technology, Technische Universitaet Muenchen,
Arcisstrasse 21, D- 80290 Muenchen, Germany

2) Remote Sensing Technology Institute, German Aerospace Center (DLR),
Oberpfaffenhofen, D- 82234 Wessling, Germany

KEY WORDS: Radar, High resolution, SAR, Satellite, Urban, Monitoring, Detection

ABSTRACT

Rising interest in traffic monitoring applications motivate the analysis of TerraSAR-X data for traffic monitoring applications. In order to sidestep the limitations of the TerraSAR-X sensor, this paper examines a new approach to improve detection using a priori information. Using Monte-Carlo Simulation the possibility of improving detection with ATI is demonstrated.

1 INTRODUCTION

1.1 Motivation

As increased traffic emerges as one of the major problems in urban and sub-urban areas, traffic-monitoring has become an increasingly important research topic. Most of the conventional systems for traffic-monitoring, however, lack of spatial extent. Hence traffic monitoring from space provides an attractive alternative to supplement existing systems. One remote sensing system to think about in this context is the upcoming TerraSAR-X Mission. Its high resolution synthetic aperture radar (SAR) sensor provides the potential for new task in remote sensing. Even more importantly the sensor can also be operated in an experimental split-antenna mode, which acquires two high resolution SAR-Images of the same scene within a small time frame. Especially this split-antenna mode is going to provide data suited for traffic monitoring. In order to determine how good the TerraSAR-X data will be suited for traffic monitoring, detection algorithms with a known measure of accuracy have to be developed.

1.2 Previous Work

The task of detecting moving vehicles with SAR sensors has been addressed in several scientific publications. In military research this problem is well known as ground moving target indication (GMTI). The method of choice in GMTI is to use a SAR sensor with at least 3 channels and use space-time adaptive processing (STAP) for target detection. Further reference to that topic can be found in (Klemm, 1998). Unfortunately space borne SAR systems with 3 or more channels are currently not available. The upcoming TerraSAR-X mission is equipped with a single channel SAR that can be switched to an experimental mode with 2 channels to enable traffic monitoring. Although the use of a 2-channel system is not optimal for detecting vehicles, some methods exist that allow detection under certain conditions. The classical method to do so is to use the displaced phase center array (DPCA) method. Along track interferometry (ATI) is another method that can be used. The issue of detecting moving targets using ATI is discussed in (Gierull, 2001). In (Gierull, 2002) special emphasis is put on the probability density functions associated with this detection. Traffic monitoring from space is quite rare so far. But as shown in (Breit et al., 2003) first endeavors have already been carried out.

1.3 Innovation

There are however a different premises to military GMTI on the one hand and civilian traffic monitoring on the other hand. In contrast to military applications, civilian applications include more constraints regarding the objects to detect. In the traffic monitoring case we can assume, that vehicles are bound to roads on a known road-network. This might not be true in military GMTI. Generally speaking, vehicles in the traffic monitoring case can be assumed to follow certain rules. These rules provide a priori information to be used for detection. It is the objective of this paper to investigate this issue. First the detection strategies are illustrated. Here special emphasis is put on the issue of incorporating a priori information into the detection. Then the possibilities of how to acquire a priori information are given, followed by a simulation quantifying these more qualitative considerations. Results of the simulation and the conclusions drawn from these results conclude the paper.

2 METHODOLOGY / THEORY

2.1 Outline of the detection method

The TerraSAR-X satellite will be equipped with a single SAR antenna of 4.8 m length that can be electronically split in 2 parts of 2.4 m each. Therefore, the sensor can be used as a 2-channel SAR with 2 antennas arranged in along-track. Both antennas observe the same surface element on ground from the same orbit position only separated by a short time lag of about $\Delta t = 0.16$ milliseconds. When relatively calibrated SAR data from each aperture are focused to a complex image (using the same matched filter for each image) and then spatially registered to each other, the image content will be identical provided the observed scene did not change within the time interval Δt. Statistical changes of the scattering properties of the earths surface and thermal noise

in the receiver of the sensor reduce the similarity of the information contained in both data sets. A measure for the similarity of the images is the coherence. It ranges from 0 (no similarity) to 1 (identical images). Due to the short time lag Δt the changes of the scattering properties are negligible. Thermal noise however reduces the coherency to an expected level of about $|\rho| = 0.95$. Objects moving in across-track direction, however, will have changed in between the two scenes, and these changes cause the following two effects in the images:

- Due to some assumptions incorporated into the SAR focusing process, an object with non-zero mean across track velocity v_y, will appear *displaced* in azimuth by a distance equivalent to the spatial shift $\Delta_{azimuth} = -Rv_{los}/v_{sat}$, with $v_{los} = v_y \cos(\theta)$, θ being the local incidence angle and v_{sat} being the satellite velocity.
- The across track velocity of the vehicle will also cause a *phase shift* ϑ, which is proportional to the targets velocity, the sensor motion and the time delay Δt

For TerraSAR-X these effects have been analyzed and quantified in more detail in (Meyer and Hinz, 2004) . These effects can be exploited in order to detect targets in SAR images. In principle, two different analytical approaches can be used to find and measure moving targets: temporal (along-track) SAR interferometry (SAR ATI), and SAR displaced phase center antenna (SAR DPCA). In this paper we will focus on the along-track interferometry approach.

2.1.1 Conventional CFAR detection In the case of along-track interferometry an interferogram I is formed from the original complex data sets I_1 and I_2 by calculating

$$\begin{aligned} I &= I_1 \cdot I_2^* = |I_1||I_2| \exp(j(\varphi_1 - \varphi_2)) = \\ &= \eta \exp(j\psi) \\ \text{with} \quad & \varphi_1 = \arg(I_1) \text{ and } \varphi_2 = \arg(I_2) \end{aligned} \tag{1}$$

For all stationary targets the interferometric phase values $\psi = (\varphi_1 - \varphi_2)$ will be statistically distributed around the expectation value $E[\psi] = 0$. The joint probability density function (pdf) $f_c(\eta, \psi)$ of amplitude and phase of an interferogram has been derived in (Lee et al., 1994) and (Joughin et al., 1994) using the underlying assumption of jointly Gaussian-distributed data in the two images. It is given by:

$$\begin{aligned} f_c(\eta, \psi) = & \frac{2n^{n+1}\eta^n}{\pi\Gamma(n)\left(1-|\rho|^2\right)} \exp\left(\frac{2n\eta|\rho|\cos(\psi)}{1-|\rho|^2}\right) \cdot \\ & K_{n-1}\left(\frac{2n\eta}{1-|\rho|^2}\right) \end{aligned} \tag{2}$$

where n is the number of looks, $\Gamma(\bullet)$ is the gamma function and $K_n(\bullet)$ is the modified Bessel function of the nth kind. As a precondition for the validity of the pdf it was assumed that $E\left[\eta^2\right] = 1$. Multilooking is done by averaging over n pixels assuming stationarity. For medium resolution SAR the jointly Gaussian assumption has been validated in most agricultural and heavily vegetated areas. Figure 1 shows a typical example of the pdf assuming a coherency of $|\rho| = 0.95$, $n = 1$ and a expected signal amplitude of $E[\eta] = 1$.
Figure 1 illustrates the typical behavior of the clutter that large phase fluctuations are associated with small amplitudes (destructive interference in the speckle patterns of the images). The phase variations are drastically reduced for large amplitudes (constructive interference in the speckle patterns of the images). The pdf is centered on a phase value of $\psi = 0$ as expected.

Based on this pdf a constant false alarm rate (CFAR) detector can be designed that groups all image pixels into two classes. Class 1, called 'clutter only', contains all pixels that only carry image information. Class 2, called 'no clutter', contains all pixels that are not part of the image pdf. This class 2 includes pixels that contain moving vehicles but also all sort of outliers. Since the pdf of this second class is not known the best thing to do is to assume it being equally distributed over a large area. With this assumption we can compute a likelihood ratio. Classification is done by comparing that likelihood ratio with thresholds α. This provides us with a curves of separation between the two classes, which are actually isolines on $f_c(\eta, \psi)$. An example of a possible curves of separation is indicated in Figure 1 by black dashed lines. The chosen curve of separation determines the probability of false alarm (P_{fa}); sometimes also referred to as "'false alarm rate"' (FAR). It is simply the integral of the Clutter pdf over the area where $f_c(\eta, \psi) < \alpha$. Thus, the FAR describes the rate of 'clutter only' pixels that are wrongly assigned to the class 'no clutter'.
Applying a CFAR detector of the given design for detecting vehicles is optimal only in cases when amplitude and phase of a possible moving target in an arbitrary image pixel is uniformly distributed. This holds for many military applications, where vehicles are not bound to roads and can move in any arbitrary direction. In case of public traffic, where a priori information about position, velocity and movement direction of vehicles is available to a certain degree, the use of a simple CFAR detector is sub-optimal.

2.1.2 Including a priori knowledge in the detection The moving target signal is assumed to have a peak amplitude β and a phase shift ϑ. The Parameter β is proportional to the square root of the radar cross section σ. A new class describing the superposition of moving target signal and clutter, called 'vehicle & clutter' can be introduced now. The Class 'vehicle & clutter' is a subset of the class 'no clutter'. Unfortunately a pdf $f_{c+m}(\eta, \psi)$ describing the probability density of this class has not been found yet. An approximation, valid for $n >> 1$ has been derived by Gierull (see (Gierull, 2002)). This approximation $f_{c+m}(\eta, \psi)$ is given by:

$$\begin{aligned} & f_{c+m}(\eta, \psi) = \\ & \frac{2n^{n+1}\eta\left(\left(\eta - \delta\cos(\psi - \vartheta)\right)^2 + \delta^2 \sin(\psi - \vartheta)^2\right)^{\frac{n-1}{2}}}{\pi\Gamma(n)\left(1-|\rho|^2\right)} \cdot \\ & \exp\left(\frac{2n\rho\left(\eta\cos(\psi) - \delta\cos(\vartheta)\right)}{1-\rho^2}\right) \cdot \\ & K_{n-1}\left(\frac{2n\sqrt{\left(\eta - \delta\cos(\psi - \vartheta)\right)^2 + \delta^2\sin(\psi - \vartheta)^2}}{1-\rho^2}\right) \\ & \text{with } \delta = \frac{\beta}{\eta} \end{aligned} \tag{3}$$

Using this approximation as an alternative hypothesis $f_{c+m}(\eta, \psi)$ allows to define a likelihood ratio. Again thresholds can be applied resulting in other curves of separation. These lines are not isolines anymore, but they separate the class 'vehicle & clutter' much better from the class 'clutter only'. Thus the risk of falsely detecting an outlier is reduced and P_{FA} is decreased. Figure 2 shows an example of the shape of $f_{c+m}(\eta, \psi)$ and its position relative to the hypotheses 'clutter only'. An example for curves of separation is also given. It encloses the class 'vehicle & clutter' much better than the one in Figure 1. The incorporation of a priori information into the vehicle detector improves the amount of detected targets and also reduces the number of false alarms. But, in order to define the 'vehicle & clutter' pdf external data sources are indispensable that allow to obtain the necessary a priori information about the vehicles impulse response β and the vehicles

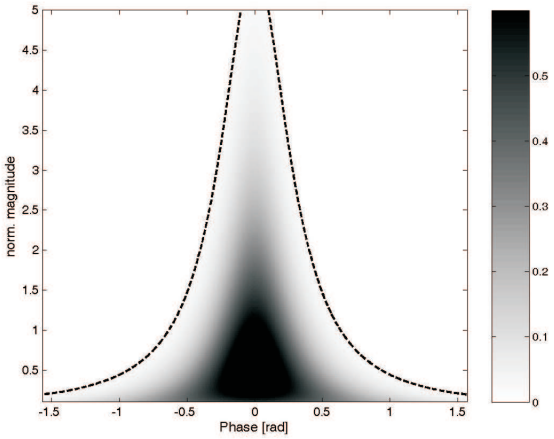

Figure 1: Theoretical joint probability density function $f_c(\eta, \psi)$ of the single-look interferometric phase and a magnitude normalized to $E[\eta] = 1$. Coherency is set to $|\rho| = 0.95$. The dashed line is an example for a curve of separation.

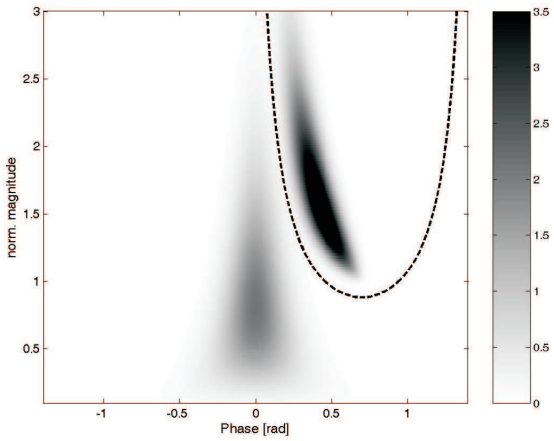

Figure 2: Theoretical joint PDF of the alternative hypotheses and its position relative to the hypotheses 'Clutter only'. The dashed line is an example for an improved curve of separation.

interferometric phase ϑ. The next section shows how to acquire that information.

2.2 How to determine a priori information

As mentioned above, one obvious and well-studied effect of moving objects in SAR-images is displacement $\Delta_{azimuth}$ in along-track direction due to an object's across-track motion. In the worst case, this would mean that a vehicle detector must be applied to the entire image. Vice-versa, assuming objects being point scatterers and given the SAR- and platform parameters, this effect can be predicted when real position, velocity, and motion direction of the mover are known. Because of the functional relation of interferometric phase ψ and object velocity in across-track direction, also the interferometric phase of a (displaced) moving object can be derived. These types of prediction may be interpreted as a priori knowledge that can be acquired, analyzed and stored independent of image acquisition. In our case, road network databases serve as basic source for acquiring a priori knowledge. Typically, these databases contain road axes in form of polygons and attributes like road class, road width, maximum velocity, etc. attached to each polygon. Using this information a number of "maps" representing the a priori information are derived (i.e. displacement map, velocity map, and interferometric phase map). Consider a vehicle hypothesis to be tested at an arbitrary image location with an approach as described in 2.1.1. Then, these maps provide information about the expected displacement from the corresponding road, the object's expected velocity, and the expected interferometric phase, which can be integrated into the hypothesis-test framework as shown above. Figure 3 shows an example for the displacement map of a single road segment. Besides the information about the phase ψ additional a priori information about the vehicles radar cross section η is necessary for determining $f_{c+m}(\eta, \psi)$. This information can again be derived using the road network. From the orientation of the corresponding road segment the aspect angle under which the car is observed by the sensor can be calculated. The dependency of the radar cross section of a car from the aspect angle is derived from simulations and experimental measurements. An example of such a curve is shown in Figure 4. The combination of both data sets enables to come up with an estimate for the most probable η that can be expected. When both parameters are derived for an arbitrary image pixel, the hypotheses 'clutter only' and 'vehicle & clutter' can be calculated and the hypotheses testing framework can be applied.

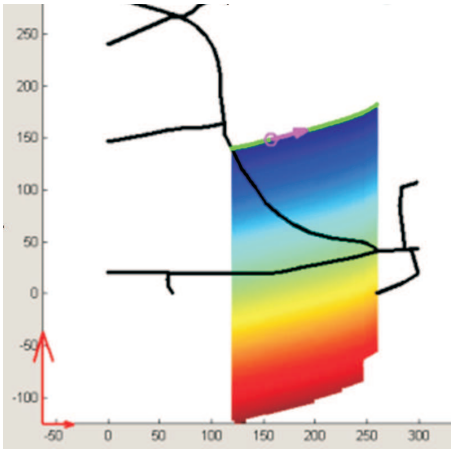

Figure 3: Example for the displacement map of a single road segment. Color is proportional to the vehicles speed.

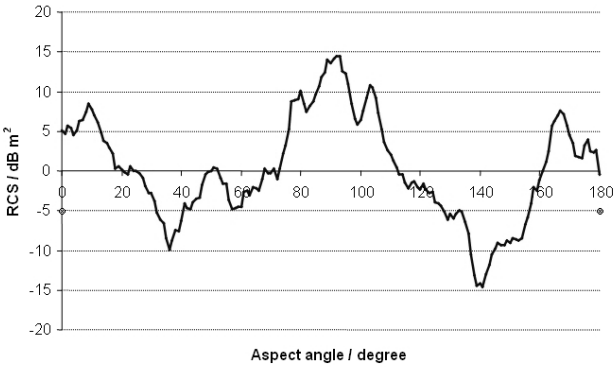

Figure 4: Radar cross section depending on aspect angle. Numerical simulation of a medium sized car in X-Band. Courtesy of Erich Kemptner, DLR-IHR.

3 IMPLEMENTATION / SIMULATION

Since the probability density functions are not known exactly for certain cases, an analytical approach turns out to be troublesome. Since TerraSAR-X has not been launched yet, there is also no real data to work with. Hence for a first approach to grasp the problem a Monte-Carlo simulation was implemented. It was cross-checked with theoretical results as far as those are known. The simulation is split into two parts: The generation of a sufficient number of random samples followed by the evaluation of these random samples. In all the simulations exact knowledge of phase and amplitude was assumed.

3.1 Generation of samples:

To generate a random sample, the whole process of data acquisition is simulated: SAR-Data-Acquisition process, multilooking, if required, and the generation of interferograms and DPCA images. Then the pixel of interest is selected and stored in a list of random samples. Two sets of random samples are created: A set with samples from a pixel containing clutter only; and a set of samples from a pixel containing the radar return of a vehicle embedded in clutter. The simulation is based on the following assumptions:

- Homogeneous Clutter
- Vehicle is modeled as a point-target
- Vehicle is moving in range with a constant velocity
- SAR-Data-Acquisition process is modeled by low pass filtering

First the parameters required for the simulation are fixed. These parameters describe the properties of the sensor, the vehicle and the clutter surrounding it. Sensor parameters were set to match TerraSAR-X specifications. Some parameters can be varied before each run of the simulation to compute different scenarios. These parameters are: Signal-to-clutter ratio (SCR), coherenceρ, speed of the vehicle considered v_{at} and the number of looks n.
Then, using these parameters, a pair of SAR-Images (I_1, and I_2) are generated. These two SAR-Images resemble the two channels of TerraSAR-X. For the sake of feasibility this is however just done for a small section around the pixel considered. When simulating both the 'clutter only' and 'vehicle & clutter' case, a pair of images containing just clutter is generated first. To do so, three images (J_1, J_2, and J_3) containing just complex gassian white noise are generated by a random generator. For the simulation to meet the right coherence ρ and backscatterer coefficient $\sigma^0 = E\left[\eta^2\right]$. They are summed as follows:

$$I_1 = \sigma^0 \left(J_1 \sqrt{|\rho|} + J_2 \sqrt{1 - |\rho|} \right) \quad (4)$$

$$I_2 = \sigma^0 \left(J_1 \sqrt{|\rho|} + J_3 \sqrt{1 - |\rho|} \right) \quad (5)$$

Then the noise is low pass filtered with a filter resembling the SAR data-acquisition process. See (Bamler and Schättler, 1993) for further reference on this topic. For the 'clutter only' case the simulation of the image ends here. For the 'vehicle & clutter' case the radar return of the vehicle without any clutter is simulated next. Two images, each containing just a point target are generated first. The magnitudes of the point targets are chosen to meet the assumed radar-cross section β of the vehicle. The phases are chosen randomly, but with a fixed phase shift ψ linking them to each other. This phase-shift depends on the vehicle's speed. Again a low-pass filter is applied to resemble the SAR data-acquisition process. Now for each channel the image containing just clutter is superimposed with the image containing just the vehicle's radar return by simply adding each pixel. This results two images for the 'vehicle & clutter case'.
We now have two simulated radar images either containing 'clutter only' or 'vehicle & clutter'. To simulate DPCA the two images are subtracted from each other to form a DPCA-image (I_d) For ATI an interferogram (I_a) is computed by multiplying the corresponding pixels of the two images. If required, multilooking can be done at this point as well. From the resulting images the samples are then collected. The simulation is repeated until the desired number of samples is reached.

3.2 Evaluation:

For each set of random samples a histogram is computed first. The two histograms are treated as a substitute for the probability density functions. There are two alternative ways of implementing the detection:
To construct a detector with a priori knowledge, a discrete likelihood function is computed by dividing the histograms element wise. Then by determining whether this likelihood is greater or smaller than a certain threshold, masks for 'clutter only' and 'vehicle & clutter' can be determined. The masks are then used to decide whether a random sample belongs to the Hypothesis 'clutter only' or the Hypothesis 'vehicle & clutter'.
The detector not considering a priori knowledge ignores the 'vehicle & clutter' histogram and just makes use of the 'clutter only' histogram. The concept of this detector follows the principle of a CFAR detector as described in section 2.1.1 A discrete likelihood function cannot be computed. Instead the threshold is directly applied to the 'clutter only' histogram. Analog to the first detector masks for both hypothesis are determined.
To evaluate the performance of the two detectors the threshold is varied and the probability of detection (P_D) and probability of false alarm (P_{FA}) are determined for each step of this variation. Then the false alarm probabilities are plotted against the probabilities of detection resulting in the so called receiver operating characteristic curve (ROC-curve).

4 RESULTS

The key question when using a priori information is: "'Are improvements possible?"' Based on the simulation explained above several ROC-curves have been computed for varying parameter sets and different detection strategies. The performance of different detection methods, namely ATI with a priori information, ATI without a priori information, DPCA with a priori information and DPCA without a priori information was evaluated based on the simulated data sets. To measure the performance, the ROC-curves of the various detectors were compared. Ideally the ROC-curve would jump up to a probability of detection of 1 right away, holding $P_D = 1$ for any P_{FA}. The opposite case - a detector just guessing - is indicated by the thin dashed line.
For DPCA the priori information, described above, is not useful in improving detection. As Figure 5 shows the ROC-curves of the two detectors are the located on top of one another; the detectors show the same performance. The comparison of the two ATI detectors shows a clear advantage for the one using a priori knowledge. For all the parameter sets examined the a priori detector yielded better results than the CFAR detector. Especially in bad detection scenarios the improvements tend to be larger. Figure 6 shows a comparison of different ROC-curves varying the signal to clutter ratio from -3db to 10db; Figure 7 shows a comparison of the two detector for different looks.

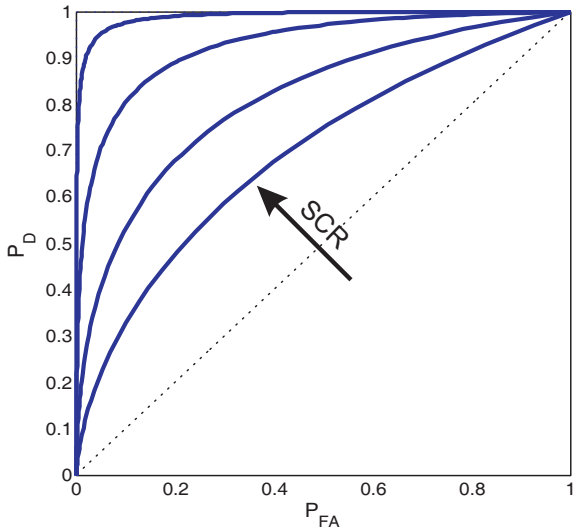

Figure 5: Performance of an DPCA-detectors for signal to clutter ratios of -3dB, 0dB, 3dB, 6dB and 10dB (innermost to outermost).

5 CONCLUSION

It has been shown, that the use of a priori information about the phase and radar cross section improves ATI detection. DPCA detection however cannot gain any improvement by this kind of a priori information. As mentioned before this simulation is just a first step to grasp the issue. Further work will incorporate inhomogeneous clutter into the simulation as well as develop a more realistic scenario of a priori information(e.g. with a distributed amplitude instead of a deterministic one).

ACKNOWLEGEMENT

This work has been founded by the DLR project "'TerraSAR-X Traffic Products"'. Special Thanks to the project members Hartmut Runge, Steffen Suchand and Michael Eineder for their support.

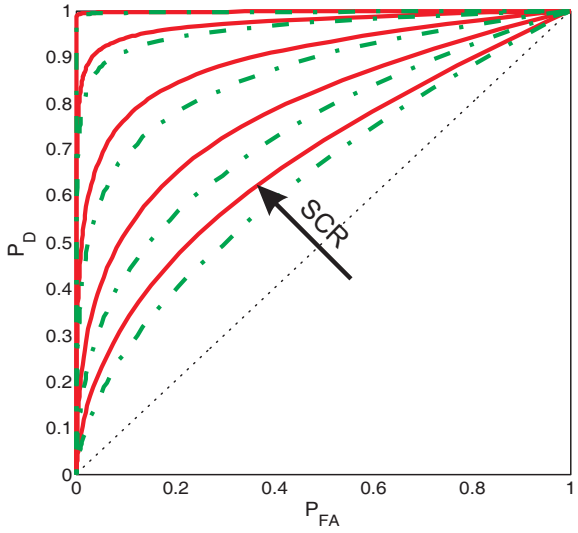

Figure 6: Performance of an ATI-detector using a priori information (solid line) compared to an ATI-detector using no a priori information (dashed line) for signal to clutter ratios of (innermost to outermost) -3dB, 0dB, 3dB, 6dB and 10dB (single look).

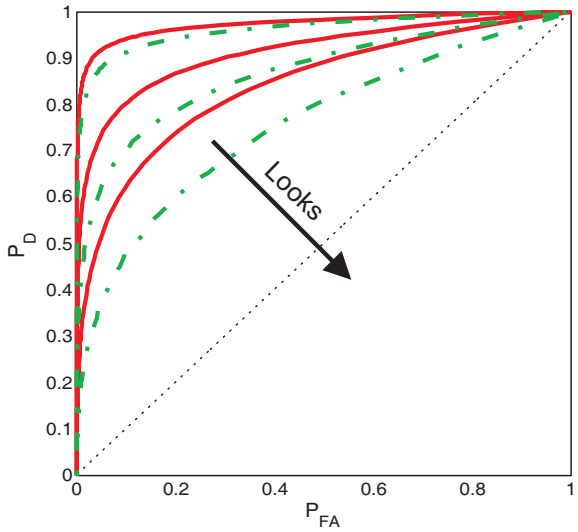

Figure 7: Performance of an ATI-detector using a priori information (solid line) compared to an ATI-detector using no a priori information (dashed line) for different numbers of looks(signal to clutter ratio fixed at 6db). From outermost to innermost: 1 look, 3 looks, 9 looks.

REFERENCES

Bamler, R. and Schättler, B., 1993. SAR Data Aquisition and Image Formation. Wichmann, Karlsruhe, chapter 3, pp. 53–102.

Breit, H., Eineder, M., Holzner, J., Runge, H. and Bamler, R., 2003. Traffic Monitoring using SRTM Along-Track Interferometry. In: IGARSS.

Gierull, C. H., 2001. Statistics of SAR interferograms with application to moving target detection. Technical Report DREO-TR-2001-045, Defence R&D Canada.

Gierull, C. H., 2002. Moving Target Detection with Along-Track SAR Interferometry. A Theoretical Analysis. Technical Report DRDC-OTTAWA-TR-2002-084, Defence R&D Canada.

Joughin, I., Winebrenner, D. and Percival, D., 1994. Probability density functions for multilook polarimetric signatures. IEEE Transactions on Geoscience and Remote Sensing 32(3), pp. 562–574.

Klemm, R., 1998. Space-time adaptive processing. The Institute of Electrical Engineers, London, United Kingdom.

Lee, J.-S., Hoppel, K., Mango, S. and Miller, A., 1994. Intensity and phase statistics of multilook polarimetric and interferometric sar imagery. IEEE Transactions on Geoscience and Remote Sensing 32(5), pp. 1017–1028.

Meyer, F. and Hinz, S., 2004. The Feasibility of Traffic Monitoring with TerraSAR-X Analyses and Consequences. In: Proceedings of IGARRS 2004.